This is a repository copy of *Graded lithium-ion battery pouch cells to homogenise current distributions and reduce lithium plating*.

White Rose Research Online URL for this paper:
https://eprints.whiterose.ac.uk/221807/

Version: Published Version

eprints@whiterose.ac.uk
https://eprints.whiterose.ac.uk/

OPEN ACCESS

Graded Lithium-Ion Battery Pouch Cells to Homogenise Current Distributions and Reduce Lithium Plating

View the article online for updates and enhancements.

Graded Lithium-Ion Battery Pouch Cells to Homogenise Current Distributions and Reduce Lithium Plating

R. Drummond,[1,z] E. C. Tredenick,[2,3] T. L. Kirk,[4] M. Forghani,[3,5] P. S. Grant,[3,5] and S. R. Duncan[2,3]

[1]*School of Electrical and Electronic Engineering, University of Sheffield, Sheffield, S1 3JD, United Kingdom*
[2]*Department of Engineering Science, University of Oxford, Oxford, OX1 3PJ, United Kingdom*
[3]*The Faraday Institution, Quad One, Harwell Campus, Didcot, OX11 0RA, United Kingdom*
[4]*Department of Mathematics, Imperial College London, London, SW7 2AZ, United Kingdom*
[5]*Department of Materials, University of Oxford, Oxford, OX1 3PH, United Kingdom*

Spatial distributions in current, temperature, state-of-charge and degradation across the plane of large format lithium-ion battery pouch cells can significantly impact their performance, especially at high C-rates. In this paper, a method to smooth out these spatial distributions by grading the electrode microstructure in-the-plane is proposed. A mathematical model of a large format pouch cell is developed and validated against both temperature and voltage experimental data. An analytical solution for the optimal graded electrode that achieves a uniform current distribution across the pouch cell is then derived. The model predicts that the graded electrodes could significantly reduce the likelihood of lithium plating in large format pouch cells, with grading increasing the C-rate at which plating occurs from 2.4C to 4.3C. These results indicate the potential of designing spatially varying electrode architectures to homogenise the response of large format pouch cells and improve their high rate performance.

Lithium-ion battery electrodes are complex non-linear dynamical systems reacting non-uniformly in space and time, especially when subject to high C-rate currents. Phenomena such as travelling wave fronts in $LiFePO_4$ (LFP) cathodes during charging[1,2] and localised lithium-plating in graphite anodes[3] are just some examples of the diverse range of non-linear behaviours that have been observed in battery electrodes, and it is these localised behaviours that often govern cell performance. To protect against these spatially localised electrochemical behaviours, the use of graded electrode structures (as in those with controlled spatial variations in electrode microstructure) has been proposed with the idea being that introducing heterogeneity into the electrode microstructure can reduce the heterogeneity in the electrochemical response.

Recently, experimental data have provided support for the use of graded electrodes in practical cells.[4] A common theme is the potential of graded electrodes to increase both the capacity at high C-rates[5,6] and the cycle life of thick electrodes,[7,8] with other benefits including a reduction in electrode tortuosity.[9] Data for both standard electrodes, such as LFP cathodes,[7,8] and non-standard electrodes, such as anodes arranged in a layered structure composed of high power $Li_4Ti_5O_{12}$ and high capacity SnO_2,[10] have shown similar benefits. However, care has to be taken when designing graded electrodes, as structuring the electrode incorrectly can deteriorate performance.[8,11] To prevent this, mathematical models have been developed to predict the electrochemical response of graded electrodes so as to quickly and cost-effectively optimize their designs. Several different models have now been developed covering a range of length scales (including micro-structural[12,13] and Doyle-Fuller-Newman-type models[2,14]) and performance metrics (such as fast charging capacitance[2] and electrical impedance[15]). These results highlight the growing maturity of battery modelling and parameterisation, which in turn, is making it increasingly straightforward to embed modelling pro-actively in the battery design process.[16] An example of this battery co-design process are the trapezoidal electrodes[7] that were developed using insights[15] on how the distribution of carbon and binder affects the conductivity of the $LiFePO_4$ electrodes.

The focus of most existing studies on graded electrodes for lithium-ion batteries has been on controlling the *through-thickness* local electrode microstructure,[12,17] including bilayer cathodes[2] composed of discrete layers of both 7D1 $Li[Ni_{0.6}Co_{0.2}Mn_{0.2}]O_2$ (NMC622) and LFP. Focusing on the through-thickness electrode structure (with experiments typically only involving coin cells[7]) is justified by the fact that it is charge mobility through the electrode thickness between the anode and cathode that governs coin cell performance. However, in recent years, there has been a general trend in commercial cells toward larger cell formats (demonstrated, for example, by the introduction of the larger 4680 cylindrical cells[18]). The idea being that larger cell formats increase the specific energy density, as the ratio of active material to superfluous materials such as casings and control circuits is increased. Large format cells have their own problems compared to coin cells; in particular, they experience new forms of spatial heterogeneities, which emerge at the macro-scale (as in across their width and length). In particular, heterogenous state-of-charge,[19] thermal hot spots[20,21] and spatially localised distributions of electrode degradation,[22–24] lithium plating,[25] and currents in-the-plane of large-format pouch cells[26,27] have been identified as impacting performance, especially in high rate applications.

The significance of in-the-plane spatial heterogeneities on the performance of large format pouch cells is becoming increasingly apparent, and has driven efforts to understand how these heterogeneities develop using mathematical models. Through these models, predictions for chemical reaction[28] and current distributions along the plane of the current collectors[29] (and how these distributions evolve with changes in the cell's design, e.g. its current collector thickness[30] and tapering[31]) have been developed, with analytical solutions even being proposed.[32] The push to understand the planar dynamics of pouch cells has meant that the number of spatial dimensions in these models has increased, with 2D[33] and 3D[21,34–38] effects often included, as opposed to the through-thickness models of, for example, the DFN model and single particle models.[39,40] One of the main drawbacks of large format battery models is their complexity, which is a consequence of their multidimensional spatial domains. This model complexity leads to several challenges including long simulation times and difficulties in model parameterisation, as discussed in the electro-thermal modelling studies.[20,21] These challenges demonstrate a need for easily

[z]E-mail: ross.drummond@sheffield.ac.uk

parameterised and computationally efficient pouch cell models able to capture the spatial distributions seen in experimental data. This problem is considered with the model introduced in Section Mathematical Model.

The formation of spatial heterogeneities across pouch cells indicates that it may be possible to grade the local electrode microstructure *in-the-plane* to mitigate their effect, similar to what has been achieved with through-thickness grading.[17,41] The graded electrode problem is illustrated in Fig. 1, with Fig. 1a indicating the planar and through-thickness directions of the pouch cell, Fig. 1b shows the simplification of the model to a 2D problem with RC circuits distributed across the plane, and Fig. 1c illustrates the 2D model domain. Fig. 1a is approximated with Figs. 1b and 1c. The model is a combination of Figs. 1b and 1c.

Contributions: In this paper, the problem of modelling and optimising graded electrode microstructures for large format pouch cells with controlled variations in resistance in-the-plane is considered. The following contributions are obtained:

1. A model for a large format pouch cells is described and validated against experimental data.[21]
2. An analytical solution for the distribution of carbon black in the electrode plane that achieves a flat current distribution across the pouch cell is derived.
3. Compared to uniform electrodes, it is predicted that graded electrodes can increase the charging rate at which lithium plating occurs from 2.4C to 4.3C.

It is proposed that a primary advantage of these graded pouch cells is to mitigate the impact of lithium plating (see Section Results: Plating Reduction with Graded Electrodes), as the flatter current distributions reduce the likelihood of negative anode overpotentials. The results highlight the importance of in-the-plane effects when characterising lithium plating in large format cells. By contrast, it is shown that the high thermal/electronic conductivity of the current collectors means that only minimal benefits of grading are observed when considering the thermal and voltage response; Section Results: Dynamic response of graded pouch cells shows that the graded cells only delivered a 1.2% increase in stored capacitance for 4C charging compared to the uniform electrodes, a conclusion in agreement with Hosseinzadeh et al., 2018.[41] These validated modelling results indicate the potential of grading to improve the cycle-life and high-rate performance of large format pouch cells. More broadly, they indicate how improvements in battery design and manufacturing could reduce the performance gap observed between coin cells constructed in laboratories and the large format cells used in commercial high-rate applications.[42]

Mathematical Model

In this section, a mathematical model of a large format pouch cell is introduced. Specific focus is given to a comparison between the model and experimental data,[21] with the presented model being simpler in form (specifically, here, circuit dynamics are used to capture the through-thickness electrical response, whereas a simple electrochemical model is used in Lin et al., 2022[21]) whilst still being able to accurately capture the in-plane spatial distributions seen in the experimental data (see Section Comparison to experimental data). Keeping the model formulation relatively simple while retaining the important physics-based mechanisms, allows analytical solutions to the optimal graded electrode design problem to be obtained (explored in Section In-the-plane electrode grading), which is the focus of this work.

Model formulation.—Figure 1 presents a schematic for the model's formulation and spatial domain. The model parameters and variables are defined in Tables A·1 and A·2. The following assumptions are made:

A1: The thicknesses of the current collectors are much thinner than their width and height.

A2: The circuit models of Fig. 1b describe the electrical dynamics at each point in the plane of the pouch cell.

A3: The multi-layer pouch cell can be modelled as an effective single layer.[20,21] **A1** is justified because large format pouch cells are considered (with typical current collector thicknesses being $\approx 10\mu m$ and their planar dimensions being $\approx$ 15cm $\times$ 20cm). Defining $i_x(y, z, t)$ as the current density through the electrode, and $I_{x,k}(x, y, z, t)$ as the current density flowing in the x-direction through current collector k, then, under this thin plate assumption, the current density gradient in the x-direction through the current collectors can be approximated by

$$\frac{\partial I_{x,k}(x, y, z, t)}{\partial x} \approx \pm \frac{i_x(y, z, t)}{L_{ck}}, \quad k \in \{n, p\}, \quad [1]$$

following the ideas of Taheri et al., 2014.[32] **A2** is a simplification of the electrode electrical dynamics, but, even so, the resulting model is able to capture the spatial distributions seen in the experimental data
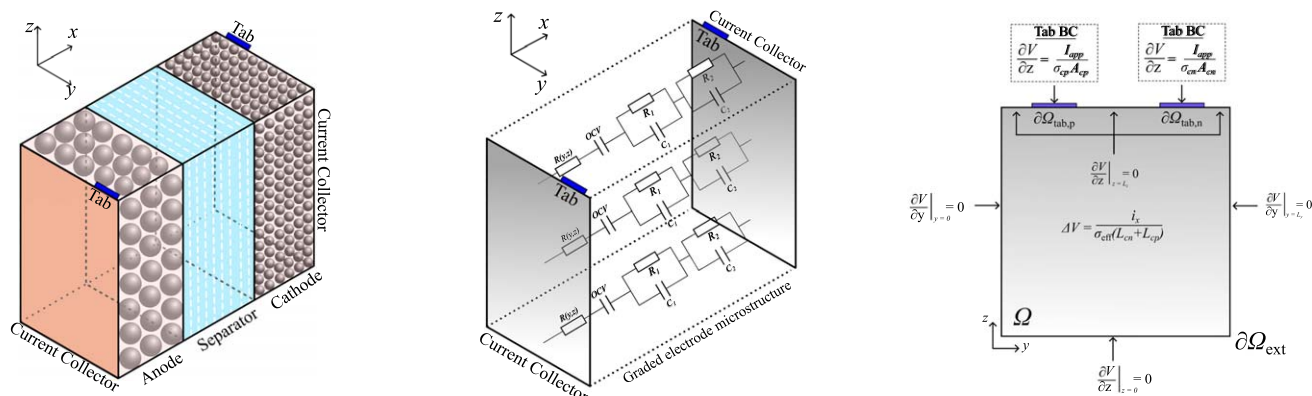
(a) Representation of electrode/separator sandwich of the pouch cell. A left handed co-ordinate system is used.

(b) Model simplification for large format pouch cells with the electrode thickness being significantly thinner than the width and length. Circuit parameters are found in Table A2.

(c) Spatial domain of the 2D pouch cell model.

Figure 1. Schematic of the 2D model for a lithium-ion battery pouch cell, Fig. 1a is approximated with Figs. 1b and 1c. The model is a combination of Figs. 1b and 1c.

(see Section Comparison to experimental data) while being simple enough to generate an analytical solution to the optimal electrode design problem (see Section Grading manufacturing). **A3** is justified under the assumption that each layer has a similar composition and so reacts similarly.

Model equations.—The following equations characterize the proposed mathematical model for large-format pouch cells, with the models domain described in Fig. 1c. Regarding the notation, each model variable in Eq. (3) is defined in the (y, z)-plane of the pouch cell, as illustrated in Fig. 1c, and may also evolve in time t. This (y, z, t) dependency of the variables is dropped in the model Eq. (3) to ease readability. $V(y, z, t)$ is the voltage (defined as the potential of the current collector at the cathode minus that of the anode) at each point in the plane, $T(y, z, t)$ is the cell temperature, $i_x(y, z, t)$ is the local through-thickness current density, $R(y, z)$ is the local resistance of the two electrodes and the separator that is constant with time, while $SoC(y, z, t)$ is the local state of charge in the plane. Table A·1 summarises the model's variables, while Table A·2 gives its parameters. For the graded cell, the only parameter varying in (y, z) is $R(y, z)$, with the rest being constants. Using the notation $\Delta f = \frac{\partial^2 f}{\partial y^2} + \frac{\partial^2 f}{\partial z^2}$ and defining

$$\sigma_{\text{eff}}(L_{\text{cn}} + L_{\text{cp}}) = \frac{L_{\text{cn}}L_{\text{cp}}}{\sigma_{\text{cn}}L_{\text{cn}} + \sigma_{\text{cp}}L_{\text{cp}}}, \qquad [2]$$

then

$$i_x = \frac{V - U(SoC, T) - v_1 - v_2}{R \, A_{\text{cell}}}, \qquad [3a]$$

$$\Delta V = \frac{i_x}{\sigma_{\text{eff}}(L_{\text{cn}} + L_{\text{cp}})}, \quad \text{on} \quad \Omega, \quad t > 0, \qquad [3b]$$

$$\rho\frac{\partial T}{\partial t} = \lambda_{\text{eff}} \, \Delta T + \frac{1}{L_x \, n_{\text{layers}}}[R \, A_{\text{cell}} \, i_x^2 - h_{\text{faces}} (T - T_{\text{ref}})], \quad \text{on} \, \Omega, \quad t > 0, \qquad [3c]$$

$$\frac{\partial SoC}{\partial t} = \frac{A_{\text{cell}}}{C_{\text{cell}}}i_x, \quad \text{on} \quad \Omega, \quad t > 0, \qquad [3d]$$

$$\frac{\partial v_1}{\partial t} = -\frac{v_1}{R_1 C_1} + \frac{A_{\text{cell}}}{C_1}i_x, \qquad [3e]$$

$$\frac{\partial v_2}{\partial t} = -\frac{v_2}{R_2 C_2} + \frac{A_{\text{cell}}}{C_2}i_x, \qquad [3f]$$

where $\Omega = [0, L_y] \times [0, L_z]$ is the projection of the cell onto the (y, z)-plane and L_y and L_z are the cell width and height, respectively. The physical meaning of Eqs. (3e)–(3f) is as follows. Equation (3a) is obtained from the circuit models[43] distributed across the plane of the pouch cell in Fig. 1b. Equation (3a) defines the through-thickness current density (as in the current density flowing across the electrodes charging the active material particles). Equation (3b) is adapted from Taheri et al.,[32] to account for the circuit dynamics and defines the distribution of the voltage in the (y, z) plane, given the current density i_x through the cell at each point. Equation (3c) defines the localised temperature dynamics of the cell and is adapted from Lin et al.,[21] with Joule heating defined from Eq. (3a) instead of electrochemical potentials.[21] Using the circuit model of Fig. 1b to describe electrical dynamics at each point (y, z) in the plane (with the derivations of these dynamics discussed in Plett[43]), Eq. (3d) describes the state-of-charge and Eqs. (3e)–(3f) are the relaxation dynamics associated with Fig. 1b's RC pairs.

Boundary conditions.—Using the notation of $n_\perp$ as the two-dimensional unitary vector normal to the boundary and $\nabla T(y, z, t) = [\partial T/\partial y, \, \partial T/\partial z]^\top$, then the model's boundary conditions are:

$$n_\perp \cdot \nabla T = -\frac{h}{\lambda_{\text{eff}}}(T - T_{\text{ref}}), \quad \text{on} \quad \partial\Omega_{\text{ext}}, \quad t > 0, \qquad [4a]$$

$$n_\perp \cdot \nabla T = -\frac{h_{\text{tab}}}{\lambda_{\text{eff}}}(T - T_{\text{ref}}), \quad \text{on} \quad \partial\Omega_{\text{tab}}, \quad t > 0, \qquad [4b]$$

$$\frac{d V}{d z}\Big|_{z=L_z} = \frac{I_{\text{app}}}{\sigma_{\text{ck}}A_{\text{tab}}}, \quad \text{on} \quad \partial\Omega_{\text{tab,k}}, \quad k \in \{n, \, p\}, \, t > 0, \qquad [4c]$$

$$n_\perp \cdot \nabla V = 0, \quad \text{on} \quad \partial\Omega_{\text{ext}}, \quad t > 0, \qquad [4d]$$

where $\partial\Omega_{\text{tab,n}}$ and $\partial\Omega_{\text{tab,p}}$ are the negative and positive tabs, $\partial\Omega_{\text{tab}} = \partial\Omega_{\text{tab,n}} \cup \partial\Omega_{\text{tab,p}}$, $\partial\Omega$ is the external boundary region and $\partial\Omega_{\text{ext}}$ is the external boundary region without the tabs, $\partial\Omega_{\text{ext}} = \partial\Omega \backslash \partial\Omega_{\text{tab}}$.

Numerical solution procedure.—To simulate the model, the partial-differential-algebraic equations of Eqs. (3) and (4) were discretised in space using Chebyshev spectral collocation[44] and solved using "ode15s" in MATLAB® 2022b.[45] On average, a 5C charge of a uniform cell took 12.7 s (with 24x24 nodes) when run on a desktop Macintosh (MacBook Pro, Monterey, v 12.4, M1 2020, 16GB, 256GB, 64 bit). The unknown model parameters were found by fitting to 4C square-wave-excitation experiments starting at 30% SOC.[21] The open-source code for the pouch cell model simulations can be found at: https://github.com/EloiseTredenick/2DBatteryTemperatureGradedModel.

Comparison to existing models: The main differences between the large-format pouch cell model of (3) and existing models[21,32] are: *i*) the inclusion of the spatially-varying resistance, $R(y, z)$, in (3), *ii*) the model's relative simplicity, with no DFN-type through thickness electrochemical modelling being used; instead, the circuit of Fig. 1b is distributed in the plane. The relative simplicity of the model is a deliberate design choice as it significantly simplifies the model parameterisation problem, which is crucial for capturing the experimental data.

It is also noted that graded planar cells were also investigated in Hosseinzadeh et al., 2018,[41] where a DFN-type model with grading both in-the-plane and through-the-thickness of the electrodes was developed. The two main differences between this paper and Hosseinzadeh et al., 2018[41] are: *i*) an analytical solution for planar graded electrodes to achieve a uniform current distribution is obtained here (see Eq. (7)), *ii*) in this paper the model predictions are validated against experimental data from Lin et al., 2022,[21] *iii*) it is proposed that the benefits of in-the-plane grading are to reduce electrode degradation (especially plating), whereas voltage and thermal considerations were considered in Ref. 41.

Comparison to experimental data.—The experimental data from Lin et al., 2022[21] is used to validate the lithium-ion battery pouch cell model of (3). Briefly, the data is obtained from square-wave-excitation cycling experiments starting at 30% state of charge (SoC), using 20 Ah pouch cells from A123 Systems with LFP positive electrodes and graphite negative electrodes, which were cycled at 4C (at currents ±80 A) for 100 seconds. A thermal imaging camera was then used to capture thermograms of the cell surface and to visualise the cell's temperature distribution across the plane during the cycling.

Model validation.—Figures 2 and 3 compares the model simulations against the experimental data[21] for cycling using the
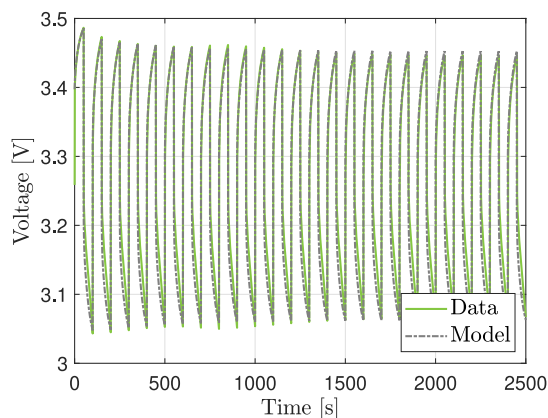
(a) Comparison between the average voltages of the experimental data and the model of (3) during cycling at 4C.
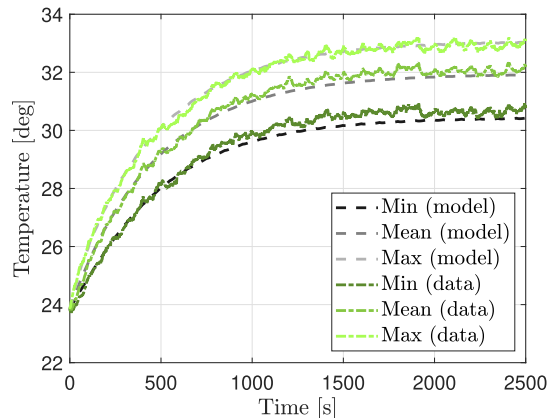
(b) Comparison of the minimum, average, and maximum temperatures across the plane of the pouch cell between the experimental data and the model of (3) at 4C.

Figure 2. Comparison between the pouch cell temperature and voltage responses of the mathematical model of (3) and the experimental data of Lin et al., 2022[21].

parameters from Table A·2. The parameters were estimated using a combination of fitting and a comparison to values from the literature, with the notation R_0 for the resistance of the uniform cell. Model agreement was observed in both the electrical and thermal response, as shown in Figs. 2a and 2b.

Figure 2b shows that the model was able to capture the evolution of the maximum, minimum, and average values of the cell temperature across the plane of the pouch cell during the cycling. A main discrepancy between the results of the model and the experimental data is that the results for the model are much smoother. The increased variability of the data is to be expected, as the sensing noise and the inherent randomness in the microstructure introduced by manufacturing limitations are not captured by Eq. (3). However, the model is still able to capture the general trends of the data, with the time constants and steady-state values of the first-order responses seen in the temperature dynamics being captured.

Figure 3 compares snapshots in the plane of the temperature distribution of the model and the experimental data,[21] where the snapshots were taken at $t =$ 100s, 500s, 1000s, and 2500s. Even though the underlying model of Eq. (3) is simple, strong agreement was made with the experimental thermal data from Lin et al., 2022[21]. In particular, the formation of a thermal hot spot as well as the general shape of the temperature contours were captured by the model, although, again, the model's diffusion dynamics resulted in smoother contours than those seen in the data. We note that Lin et al., 2022[21] presented a 3D model solved in COMSOL for the same data and a similar fit to that of Fig. 3 was achieved. Therefore, even though the model of Eq. (3) is arguably simpler than that of Lin et al., 2022[21] (see Section Numerical solution procedure for details), a similar level of model accuracy could be achieved.

Figure 4 illustrates how the validated model can be used to infer the impact of design changes in the pouch cell on the degree of spatial heterogeneity across the plane. Defining the variation in the current density as the difference between the maximum and minimum current density across the plane, Fig. 4a shows how this variation changes with resistance (as in, with $R(y, z) = R_0$), Fig. 4b shows how it changes with pouch cell length, and Fig. 4c shows how it changes with current collector thickness. The Fig. identifies some near linear relationships between these cell parameters and the variation in current density (Fig. 4 b), or its inverse (Figs. 4a and 4c), with explicit characterisations for these expressions obtainable from the analytical solution of Taheri et al., 2014.[32] As could be expected, the Fig. indicates that the variation of the current distribution across the pouch cell increases as: *i)* the cell resistance decreases, *ii)* the aspect ratio increases, and *iii)* the current collectors get thinner.

Notably, Fig. 4a suggests that as the cell ages, and so as its resistance increases, the variation in current distribution across the cell is likely to decrease, as more current is encouraged to flow along the current collectors rather than through the thickness of the cell.

In-the-plane Electrode Grading

The spatial distributions seen in the response of the pouch cell, for example in the temperature data of Fig. 3, presents an opportunity to apply electrode grading to create a more uniform electrochemical response. In this section, an analytical solution for the resistance distribution across the plane of the pouch cell, $R(y, z)$, to achieve a uniform current distribution is described.

Grading manufacturing.—It is assumed that the electrode resistance $R(y, z)$ can be controlled locally in space. The reasons for focusing on the resistance distribution are: *i)* following Eqs. (3a) and (3b), the electrode resistance $R(y, z)$ directly influences the current distribution across the pouch cell (and it is variations in the current which are targeted to be smoothed out by the optimally graded electrode), *ii)* existing results on through-thickness electrode grading have demonstrated how this resistance grading can be achieved, e.g. by controlling the relative mass fraction of carbon black in LFP cathodes using spray printing techniques.[15] Achieving in-plane grading of electrodes using conventional techniques can be challenging. However, innovative methods such as spray printing show promise for creating a gradient across the thickness of electrodes. This technique can also effectively apply grading across the plane of the electrode. While spray printing has potential, it is currently limited to small-scale applications. In contrast, traditional methods like slurry casting can be creatively adapted to achieve partial in-plane grading.[7,8] In future research, we will present experimental data on in-plane graded LFP electrodes fabricated using both spray printing and modified slurry casting techniques.

Resistance distribution for homogeneous current.—The problem of distributing the resistance (achieved by controlling the weight fraction of active carbon in the electrode microstructure) to achieve homogeneous current distribution across the pouch cell is considered. This targeted flat current distribution is equal to the average current density, with

$$i_x(y, z, t) = \frac{I_{\text{app}}(t)}{A_{\text{cell}}}. \quad [5]$$

Equation (3) implies that, under isothermal conditions of the open-circuit voltage, if a uniform current distribution is achieved at $t = 0$,

(a) Model: $t = 100$s.

(b) Data: $t = 100$s.

(c) Model: $t = 500$s.

(d) Data: $t = 500$s.

(e) Model: $t = 1000$s.

(f) Data: $t = 1000$s.

(g) Model: $t = 2500$s.

(h) Data: $t = 2500$s.
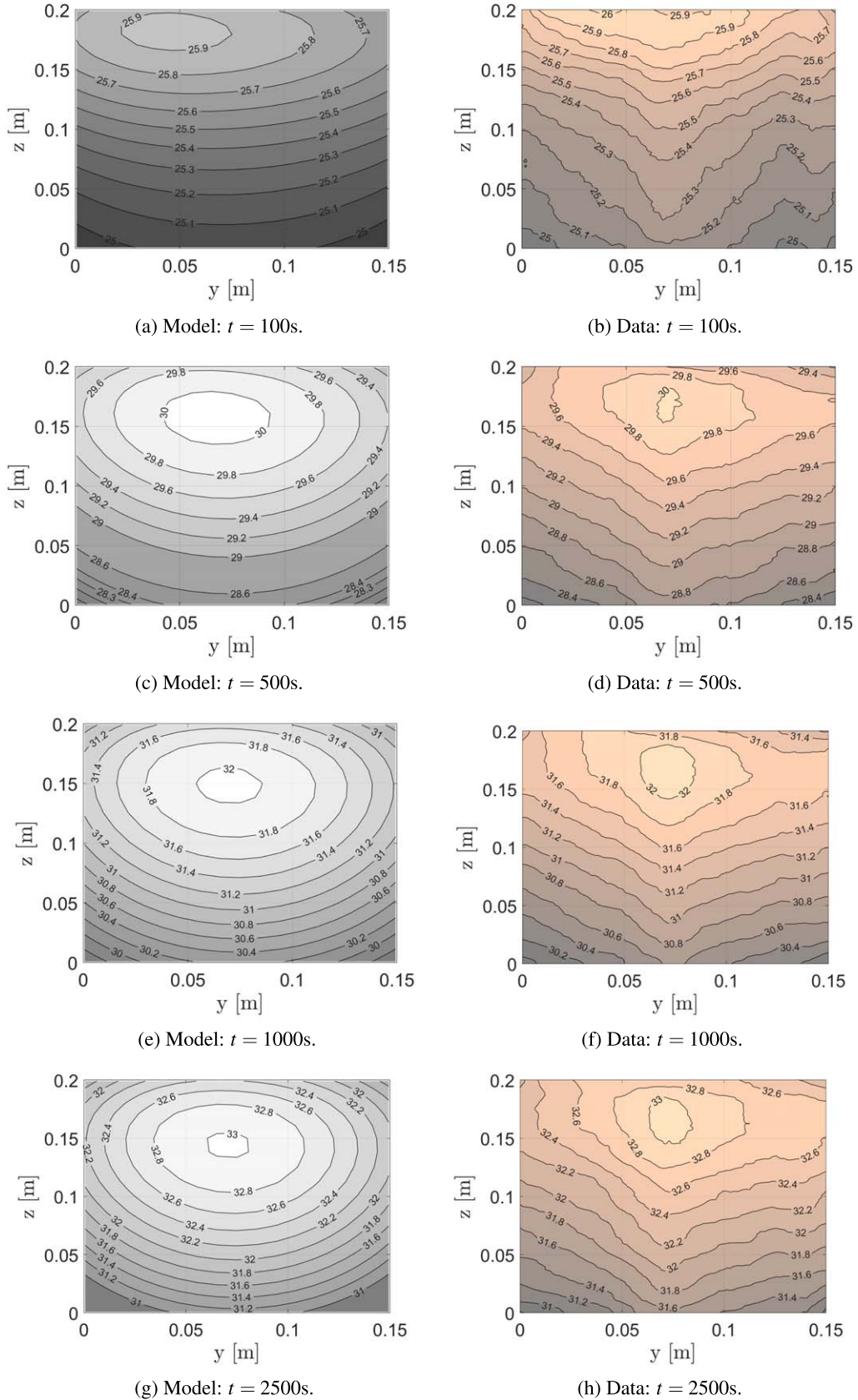
Figure 3. Temperature distributions across the plane of the pouch cell. Comparison between the model of (3) and the experimental data. Snapshots at $t = 100$s, 500s, 1000s and 2500s are shown.

then v_1, v_2 and the SoC, will evolve uniformly in space as well. The implication is that if the current distribution is uniform at $t = 0$, it will remain uniform during the simulation, following the model equation

of (3a) and (3b), which may not hold exactly in practice as local current spikes might emerge caused by the variability in the local electrode composition. However, this can be used to simplify the

graded electrode design optimisation problem, and smooth out current and temperature gradients across the pouch cells. Specifically, it converts a dynamic optimisation problem into a static one, in the sense that it changes the optimisation from one of determining how the resistance should be distributed to achieve a uniform current distribution during the whole charge to one that only has to consider the distribution at the start of the charge. A consequence of this problem formulation is that it allows an analytical solution to the graded electrode design optimisation to be derived (see Eq. (7)).

Problem formulation.—The desired uniform current distribution of Eq. (5) is substituted into Eqs. (3a) and (3b) to give, after simplifying,

$$\Delta R - \frac{1}{A_{\text{cell}} \sigma_{\text{eff}}(L_{\text{cn}} + L_{\text{cp}})} = 0, \quad \text{on } \Omega, \qquad [6a]$$

which is a non-homogeneous Laplace equation in the spatial variable $R(y, z)$. Using the same approach, the boundary conditions for the voltages from Eqs. (4c) and (4d) can be translated into boundary conditions for the resistance to achieve a uniform current density, as in

$$\frac{\partial R}{\partial z}\Big|_{z=L_z} = \frac{1}{\sigma_{\text{ck}} A_{\text{tab},k}}, \quad \text{on } \partial\Omega_{\text{tab},k}, \ k \in \{n, p\}, \qquad [6b]$$

$$n_\perp \cdot \nabla R = 0, \quad \text{on } \partial\Omega_{\text{ext}}. \qquad [6c]$$

Solution.—The solution to Eq. (6) is

$$R(y, z) = R_{\text{quad}}(z) + R_{\text{hyper}}(y, z) \qquad [7a]$$

composed of a quadratic part, $R_{\text{quad}}(y, z)$, and a hyperbolic part, $R_{\text{hyper}}(y, z)$, satisfying

$$R_{\text{quad}}(z) = d_0 + d_1 z + d_2 z^2, \qquad [7b]$$

$$R_{\text{hyper}}(y, z) = \sum_{n=0}^{\infty} c_n \cos\left(\frac{n\pi y}{L_y}\right) \cosh\left(\frac{n\pi z}{L_y}\right). \qquad [7c]$$

The coefficients of this solution are

$$d_1 = 0, \qquad [7d]$$

$$d_2 = \frac{1}{2 \, A_{\text{cell}} \ \sigma_{\text{eff}} \ (L_{\text{cn}} + L_{\text{cp}})}, \qquad [7e]$$

$$c_n = \frac{2}{n\pi \, \sinh\left(\frac{n\pi L_z}{L_y}\right)} \int_0^{L_y} h(y) \cos\left(\frac{n\pi y}{L_y}\right) \, dy, \qquad [7f]$$

with

$$h(y) = \begin{cases} -\dfrac{L_z}{A_{\text{cell}} \sigma_{\text{eff}}(L_{\text{cn}} + L_{\text{cp}})} & y \in \Omega_{\text{ext}}, \quad z = L_z, \\[2mm] \dfrac{1}{\sigma_{\text{c1}} A_{\text{tab},1}} - \dfrac{L_z}{A_{\text{cell}} \sigma_{\text{eff}}(L_{\text{cn}} + L_{\text{cp}})} & y \in \Omega_{\text{tab},1}, \quad z = L_z, \\[2mm] \dfrac{1}{\sigma_{\text{c2}} A_{\text{tab},2}} - \dfrac{L_z}{A_{\text{cell}} \sigma_{\text{eff}}(L_{\text{cn}} + L_{\text{cp}})} & y \in \Omega_{\text{tab},2}, \quad z = L_z, \end{cases}$$

$$[7g]$$

and the constant d_0 being a free variable setting the average value of the resistance. This resistance distribution defines the graded electrodes of the following analysis. To evaluate Eq. (7c), the infinite sum has to be truncated after a finite number of terms. It was found that a truncation of the order of 20 terms was sufficient to achieve a stable and accurate solution.

The solution of Eq. (7) shows that the resistance should roughly decrease away from the tabs in order to flatten the current distribution. The physical meaning of decreasing the resistance away from the tabs is to encourage current to flow down the length of the current collectors, instead of going directly through the electrodes as it enters one of the tabs and leaves the other. In the particular setup of Fig. 1 and Table A·2, where the cell has a relatively high aspect ratio, the variation of the resistance is much larger in the z-direction rather than the y-direction, but, following Eq. (7), this may change for wider cell formats or for different tab configurations.

Results: Flat current distribution across pouch cells.—Figure 5 compares the current and resistance distributions achieved with both uniform and graded pouch cells (with the resistance of the graded cells following the solution derived in Eq. (7)). For this analysis, both pouch cells had equal average resistances of $1.5 \times 10^{-3}\Omega$ to ensure a fair comparison. Significant variation was seen in the current density distribution of the uniform cell (with a maximum value of 3925 A m^{-2} at the tabs and a minimum value of 2138 A m^{-2} at the opposite end where $z = 0$). By contrast, the graded cell achieved a constant current density of 2667 A m^{-2} across the plane, as predicted.

Regarding whether the optimised resistance distributions of Fig. 5 could be realised in practice, consider the maximum change in resistance that could be achieved by changing the local weight

(a) Current variation with resistance.

(b) Current variation with length.

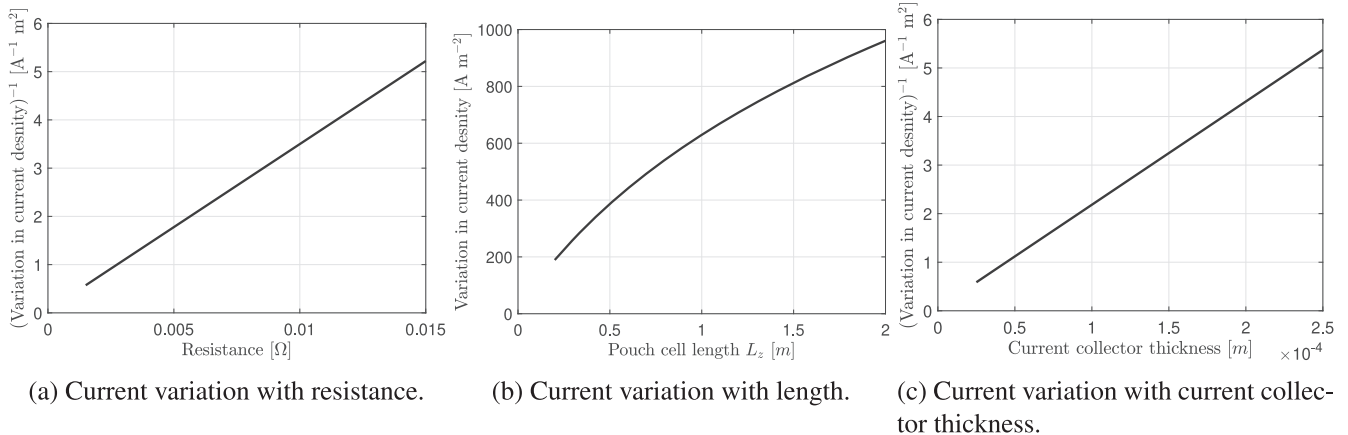(c) Current variation with current collector thickness.

Figure 4. Variation of the current distribution (difference between its maximum and minimum) with pouch cell resistance, length, and current collector thickness.
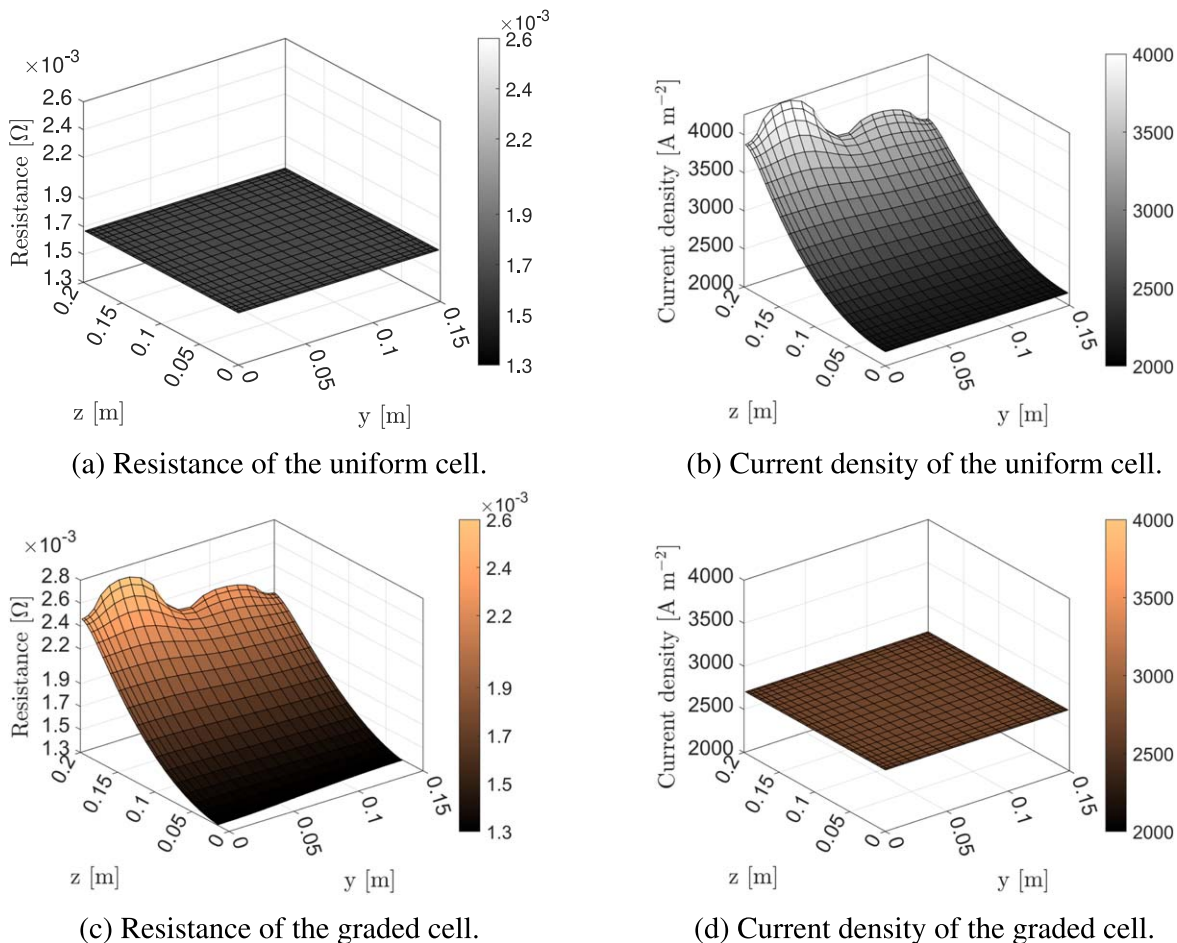
(a) Resistance of the uniform cell.

(b) Current density of the uniform cell.

(c) Resistance of the graded cell.

(d) Current density of the graded cell.

Figure 5. Distributions in resistance and current density of the graded and uniform cells after a 4C charge. The uniform cell has a constant resistance, but a spatially varying current distribution. The graded cell has a spatially varying resistance, but a constant current distribution.

fraction of carbon black in the LFP cathodes. The characterization of electronic conductivity of LFP cathodes in terms of the weight fraction of carbon black, w_{cb}, from Drummond et al.,[15] is assumed. The resistance of the LFP cathode, R_{LFP}, is approximated[15] by

$$R_{LFP} = \frac{\ell}{n_{layers} A_{cell} \sigma_\infty w_{cb}{}^b} \qquad [8]$$

where $\sigma_\infty = 4.01$ S m^{-1}, $b = 1.7$, and the electrode thickness is $\ell = 100\ \mu$m. Define $\overline{R}_{LFP}$ as the maximum resistance in Fig. 5 (with a weight fraction of carbon black of $\overline{w}_{cb}$) and $\underline{R}_{LFP}$ as the minimum resistance (with a weight fraction of carbon black of $\underline{w}_{cb}$). Note that $\underline{w}_{cb} > \overline{w}_{cb}$ since carbon black increases the conductivity of the LFP electrode. The difference between the maximum and minimum resistances of the graded design is $\overline{R}_{LFP} - \underline{R}_{LFP} \approx 1.2 \times 10^{-3}\ \Omega$. Therefore, the differences between the two weight fractions satisfies

$$\frac{1}{\overline{w}_{cb}{}^b} - \frac{1}{\underline{w}_{cb}{}^b} = \frac{n_{layers} A_{cell} \sigma_\infty (\overline{R}_{LFP} - \underline{R}_{LFP})}{\ell}. \qquad [9]$$

If the weight fraction of carbon black in the LFP cathode at the point with minimum resistance is $\underline{w}_{cb} = 0.06$, then Eq. 9 implies that the weight fraction at the point with maximum resistance should be $\overline{w}_{cb} = 0.0471$. This is a modest difference and readily achievable in practice. Subtle changes in the electrode microstructure, for example in the distribution of carbon black in LFP cathodes, can therefore significantly influence how heterogeneities emerge across pouch cells.

Results: Dynamic response of graded pouch cells.—Figure 6 compares the optimised graded electrode cell following Eq. (7) and

the uniform cell for a full 4C charge at $I_{app} = 80$A. Figure 6 provides justification for the design choice of Section Grading manufacturing, which optimises the spatial resistance of the pouch cells to achieve a uniform initial current distribution in space, as Fig. 6a implies that this uniformity in the current was retained during the whole charge. By contrast, the current distribution in the uniform cell is more variable. Initially, large current gradients exist across the plane of the uniform cell, as shown in Fig. 6a, with the maximum current density 3925 A/m^{-2} at the tabs and the minimum current 2138 A/m^{-2} at the opposite end. The non-uniform current distribution then causes the voltage to vary, following Eqs. (3d)–(3f). Simultaneously, there is a negative feedback effect acting on the voltages from Eqs. (3a) and (3b) that smooths this variation. The interactions between these two modes causes the spatial distribution of the current to evolve in both space and time. In particular, Fig. 6a shows that the current does not change significantly during 100s $\leqslant t \leqslant 450$s when the OCV curve is flat (since the smoothing effect of U in Eq. (3a) is not active). It is this smoothing effect that causes the region near the tabs to charge first, but then, when it is fully charged, the majority of the current then flows through the bottom half of the cell.

Figure 7 shows snapshots of the current distribution across the current collectors of the pouch cell with uniform electrodes at $t = 1$s, 200s, 500s and 600s during the 4C charge. At the start of the simulation, the peak current was at the tabs, with this peak moving down the cell during the charge. It is noted that the maximum variation in the current distribution in the plane was recorded near the end of the charge, which is also the time when lithium-plating is most likely to occur.

Whilst Fig. 6a implies that there would be large differences between the current distributions of the uniform and graded cells,
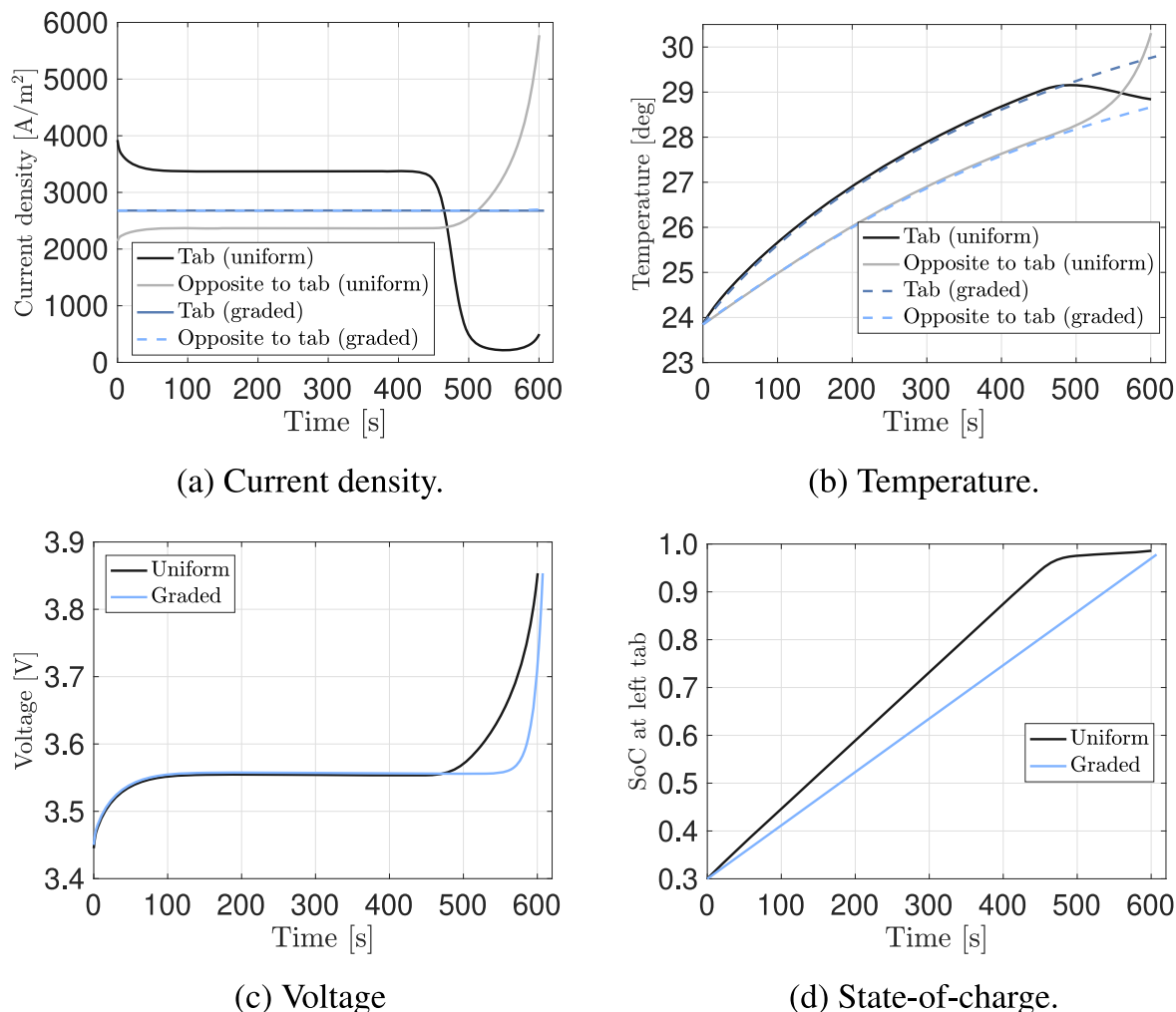
(a) Current density.

(b) Temperature.

(c) Voltage

(d) State-of-charge.

Figure 6. Spatial-heterogeneity of the model's variables, including state-of-charge, temperature, voltage and current density during a 4C charge. The difference between these variables at the tabs and opposite the tab is shown.

Figs. 6b and 6d indicate that the impact of these differences on the variable *internal* to the current collectors would actually be quite limited. Specifically, Fig. 6b compares the temperatures, Fig. 6c the voltages, and Fig. 6d the state-of-charges. Although there are some differences between the uniform and graded electrodes, it is relatively limited compared to the large variations seen in the current distributions. In particular, even though the profiles of the two voltage curves in Fig. 6c are different, they reach the cutoff voltage of 3.85 V at approximately the same time (607s for the graded cell and 600s for the uniform one). As such, the capacitance improvement of the graded cell over the uniform one is only 1.2%. These limited gains in the capacitance are a result of the large thermal and electrical conductivities of the current collectors (see Table A·2), which smooth out the variations in the electrodes responses across the plane. Similarly, for the current, Appendix Figure A·1 compares the modelled 4C cycling results for the graded and uniform cells. The current density of the graded cell is close to $I(t)/A_{cell}$, while the uniform cell has large variations both in time and across the plane. By contrast, the maximum temperature is slightly reduced by 0.3 °C for the graded cell.

When only variables defined internally to the current collectors (such as temperature and voltage) are used to assess the value of graded pouch cells, their benefits may be lost. This observation agrees with the conclusions of Hosseinzadeh et al., 2018[41] that porosity distribution through the electrode thickness has the potential to produce superior battery performance instead of when the porosity is varied along the electrode height. However, in this paper, it is proposed that to unlock

the benefits of graded pouch cells, a performance metric that focuses on *through-thickness effects* should instead be considered. This observation motivates the analysis of the following Section on the potential benefits of graded electrodes to mitigate lithium plating.

Results: Plating Reduction with Graded Electrodes

The potential of graded electrodes to mitigate lithium plating in large format cells is explored in this section. As discussed in relation to Figs. 6b–6d and in the results of Hosseinzadeh et al., 2018,[41] it was observed that the high conductivity of the current collectors limits the apparent value of electrode grading in-the-plane when only variables found "*internally*" to the current collectors (with *internal* variables being understood as those, such as voltage and temperature, that are smoothed out when flowing in the plane of the current collectors) are used to assess performance, as opposed to variables flowing through the electrodes (such as the current distributions of Figs. 7 and 6a). However, as lithium plating is a localised degradation phenomenon dependent upon the charging current and electrochemical state of the electrode at a given point, it is shown in this Section that plating may be effectively mitigated by in-the-plane electrode grading. The focus toward mitigating lithium plating is also motivated by experimental studies[25] which show significant spatial variations in plating across graphite anodes. Controlling the distribution of active carbon in the electrode microstructure to mitigate the spatial distribution in plating is proposed as a means to reduce the accelerated degradation of large format pouch cells in high-rate applications.
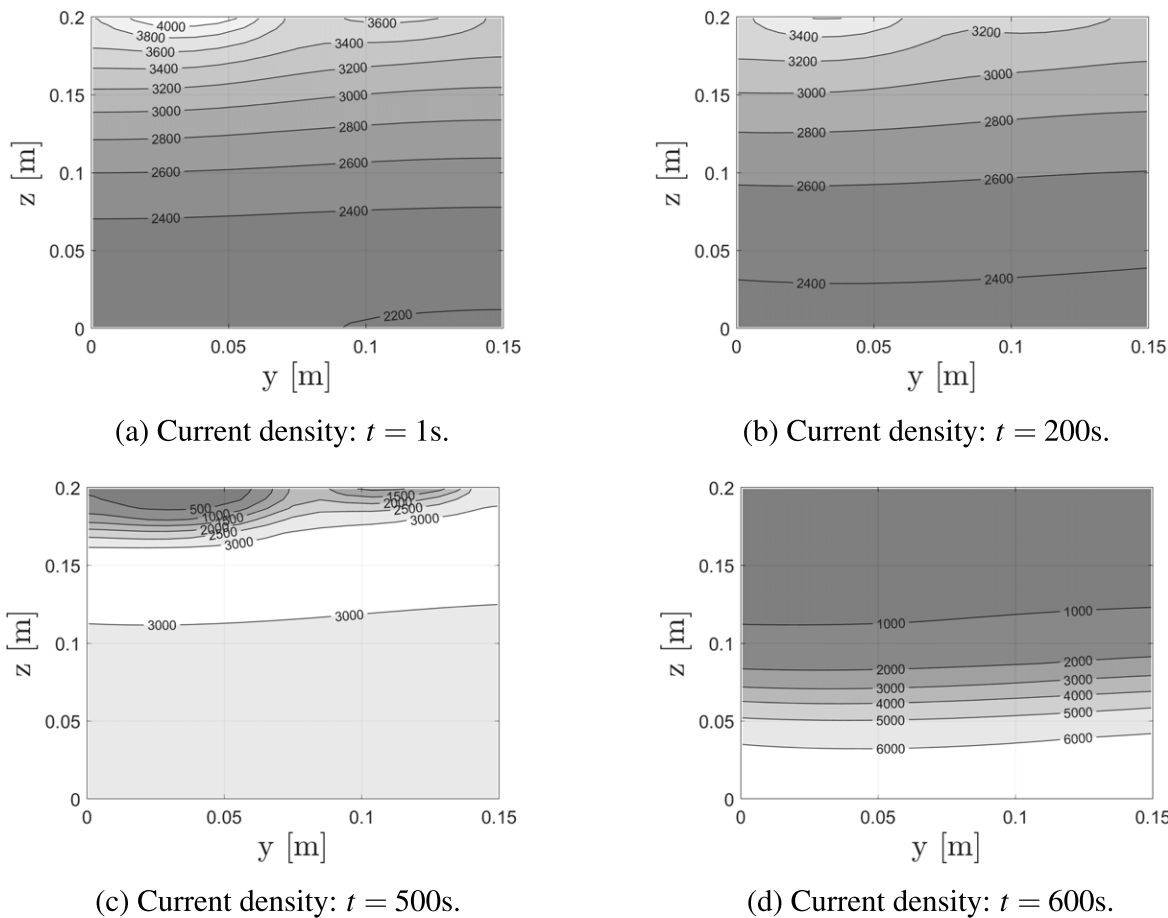
(a) Current density: $t = 1$s.

(b) Current density: $t = 200$s.

(c) Current density: $t = 500$s.

(d) Current density: $t = 600$s.

Figure 7. Current density distributions in the plane of the uniform pouch cell using the model of Eq. (3) during a constant current charge at 4C. Contour lines indicate current density values in A m^{-2} going through the electrode sandwich. The location of maximum current travels from the tabs to opposite them during the charge.

(a) C-rate dependency of plating.

(b) Plating onset during 5C charging.
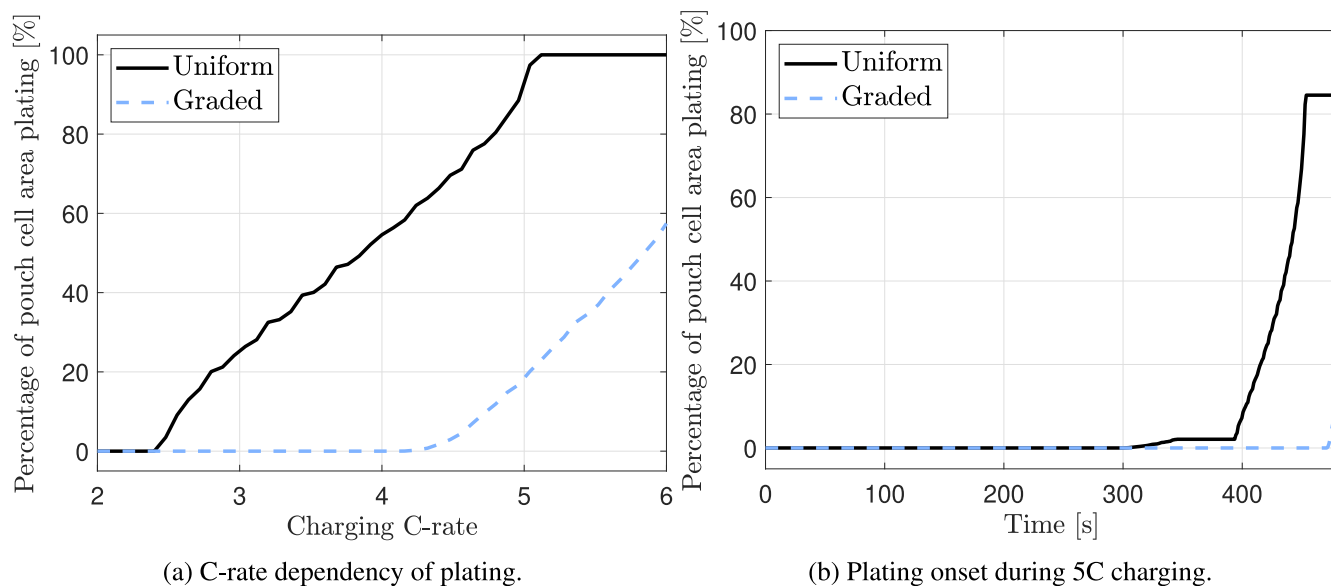
Figure 8. Comparing the onset of lithium-plating between the uniform and graded pouch cells. Figure 8a shows the C-rate dependency of the plating and Fig. 8b compares the progression of plating during 5C charging.

A mathematical modelling approach was used to compare the extent of lithium plating between the graded and uniform cells. However, modelling lithium plating is known to be challenging, with existing models typically being additions to complex electrochemical models, with example models discussed in Ref. 46, 47. By contrast, in this paper, a simpler, control-orientated model adapted from[48] was used, with this model based off of the earlier results of.[49] For the state-constrained control problem considered in Ref., 48 the following
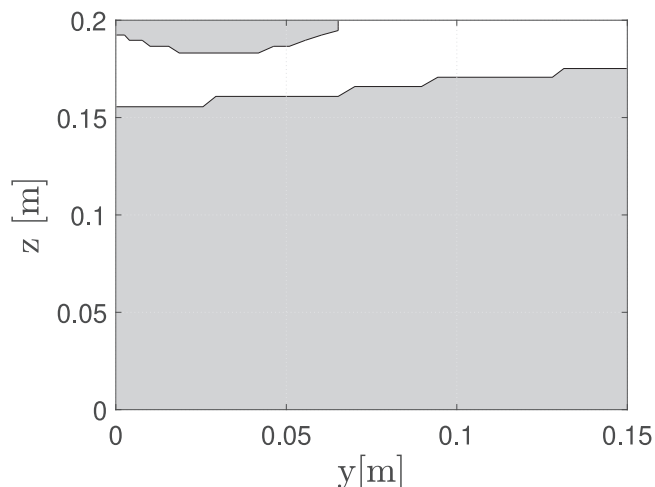
Figure 9. Distribution of plating across the plane at the end of a 5C charge of the uniform cell. The gray region has experienced plating and the white region is free of plating.

condition for lithium plating was developed, with the anode regarded as experiencing plating if the following inequality is satisfied

$$a_{\text{lp}} \log(b_{\text{lp}} \text{SoC}(y, z, t)) + c_{\text{lp}} + d_{\text{lp}} i_x(y, z, t) \geq 0. \qquad [10]$$

The plating inequality[48] of Eq. (10) was determined by fitting a curve when the anode over-potential in a DFN model went negative. Here, $a_{\text{lp}} = 1.74$, $b_{\text{lp}} = 9.32$, $c_{\text{lp}} = -4.46$, following,[48] and $d_{\text{lp}} = 0.0055$.

Figure 8 compares the onset of lithium-ion plating for both the uniform and graded pouch cells using Eq. (10). The purpose of this Fig. is to illustrate the spatial, temporal and C-rate dependence of plating, and how modelling can capture the heterogeneity of pouch cell degradation. For this simulation, the temperature dependency of the onset of lithium plating was neglected as it was assumed that the temperature of the cell was approximately constant. This assumption could be relaxed using more complex plating models than Eq. (10), such as those discussed in Reniers et al.,[47] as the likelihood of plating is known to increase as the cell temperature decreases, especially for sub zero temperatures.[50] Figure 8a shows the areal percentage of the pouch cell experiencing plating during charging at different C-rates. The uniform pouch cell sees a gradual increase in the area of the pouch cell experiencing plating when the C-rate is increased beyond 2.4C, with 100% of the pouch cell experiencing plating at 5.1C. By contrast, the graded pouch cell experiences no plating until 4.3C. The differences between these two curves is due to variation in the current distribution of the uniform cell; this variation leads to higher current spikes and so a greater likelihood of plating. By contrast, the model predicts that the flatter current distribution of the graded pouch cell can delay the onset of plating until a critical point is reached, and, at that point, the flat distributions cause the whole plane to plate. The predicted critical predicted C-rates for lithium plating are broadly consistent with the experimental literature; for example, Burns et al.,[51] detected plating in 220 mAh Li[Ni$_{1/3}$Mn$_{1/3}$Co$_{1/3}$]O$_2$/graphite 402035-size pouch cells at approximately 1C and 30 °C. The significance of Fig. 8a is that it suggests grading pouch cells could increase the maximum charging C-rate for which plating can be avoided. In other words, grading in the plane could increase the operating envelope of pouch cells such that they could be fast charged without suffering from plating.

Figure 8b shows the time when plating is initiated during a 5C charge. During this charge, the graded cell does not plate whereas the uniform electrodes experiences plating at the end of charge. The propensity of plating to occur in uniform cells at the end of charge is one of the main reasons why optimal fast charging currents are often tapered at the end of charge.[52,53]

Figure 9 illustrates the spatial distribution of plating across the plane of the uniform pouch cell at the end of the 5C charge. The gray area indicates a region where plating is predicted to occur. The Fig. suggests that, for these cells, most of the plating occurs opposite the tabs with the plating then progressing up the plane. This effect is in response to the current distribution being highest at the tabs at the start of the charge, causing the active particles in this region to be charged first. When these particles become fully charged, they hinder further charging in this region and so cause current to flow down toward the bottom of the pouch cell later on during the charge. By restricting the area where the current can flow through, the local current densities in this region at the bottom of the cell are increased (see also Fig. 6a), causing a higher likelihood of plating.

Conclusions

A model for large format lithium-ion battery pouch cells with spatial grading across the plane was developed and validated against experimental data. An analytical solution for the optimal electrical resistance distribution across the plane of large format pouch cells to achieve a flat current distribution was derived. The main benefit of graded electrodes identified was to increase the allowable charging C-rate from which lithium plating could be avoided; the graded electrodes increased the safe charging rate from 2.4C to 4.3C. By contrast, only a 1.2% increase in charging capacity was achieved for 4C charging. These results indicate the potential of in-the-plane graded electrode microstructures for enabling fast charging of large format pouch cells that by limiting the spatial heterogeneities. Future work will focus on experiments to fabricate graded electrodes for LFP pouch cells and validate the results of this modelling work.

Code Availability

The open-source code for the pouch cell simulations that have been used to produce the results of this study are available online (https://github.com/EloiseTredenick/2DBatteryTemperatureGradedModel).

Appendix

The open circuit voltage (OCV) function for the LFP cells[21,54] at 0.02 C is modelled by:

Table A·1. Variables of the model.

| Variable	Description	Unit
i_x	Current density through electrode thickness	A m^{-2}
I	Current density in the current collector	A m^{-2}
I_{app}	Applied current	A
I_{sign}	Sign of the current	
R	Cell series resistance	Ω
SoC	Local state of charge	—
T	Temperature	K
t	Time	s
U	Open circuit voltage (OCV)	V
V	Voltage	V
v_1	Voltage across RC-pair	V
v_2	Voltage across RC-pair	V
x	Direction through cell	m
y	Direction along cell width	m
z	Direction along cell height	m
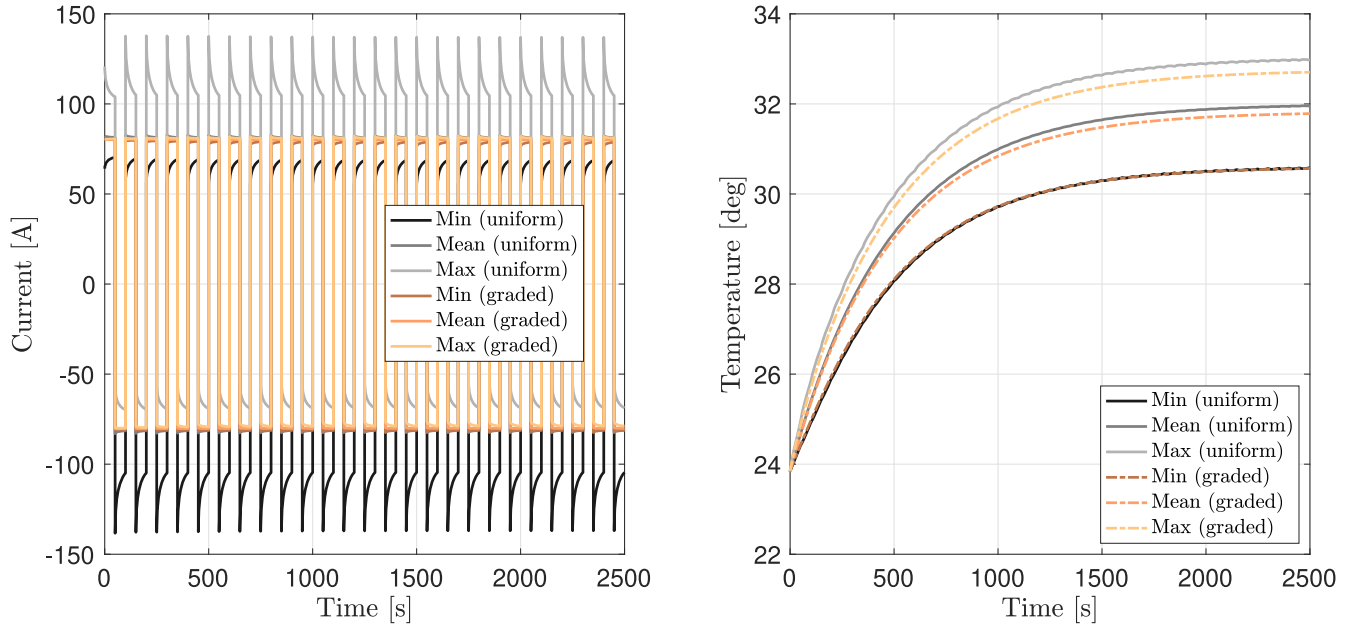
Figure A·1. Comparison between the graded and uniform models during cycling at 4C and an applied current of 80 A. The current and temperature responses with time are shown, including the minimum, average, and maximum temperatures across the plane of the pouch cell.

Table A·2. Model parameters. Experimental values obtained from[21] for an 80Ah capacity cell.

Parameter	Description	Units	Value	Source
A_{tab}	Area of a tab	m^2	1.56×10^{-4}	Experiment
A_{cell}	Cell area ($L_y \times L_z$)	m^2	30×10^{-3}	Experiment
n_{layers}	Number of electrode layers in cell		42	Experiment
C_{cell}	Capacity of cell (20 Ah) per cell area	A s	20×3600	Experiment
C_1	Capacitance of RC-pair	F	2.79×10^4	Fitting
C_2	Capacitance of RC-pair	F	8.89×10^3	Fitting
h	Heat transfer coefficient	$W\,m^{-2}\,K^{-1}$	13.2	Fitting
h_{tab}	Heat transfer coefficient of tabs	$W\,m^{-2}\,K^{-1}$	51.58	Fitting
h_{faces}	Effective heat transfer coefficient of current collector faces	$W\,m^{-2}\,K^{-1}$	$210 \times L_x$	Fitting
L_{cn}	Thickness of negative current collector in x direction	μm	25	Experiment
L_{cp}	Thickness of positive current collector in x direction	μm	25	Experiment
L_x	Electrode thickness	m	110×10^{-6}	Experiment
L_y	Height of battery	m	0.2	Experiment
L_z	Width of battery	m	0.15	Experiment
R_0	Series resistance of Uniform cell	Ω	1.5×10^{-3}	Fitting
R_1	Resistance of RC-pair	Ω	1.10×10^{-3}	Fitting
R_2	Resistance of RC-pair	Ω	2.25×10^{-4}	Fitting
T_{ref}	Constant absolute reference temperature	K	298.15 (25 °C)	Experiment
λ_{eff}	Effective thermal conductivity	$W\,m^{-1}\,K^{-1}$	4.5	Fitting
ρ	Volumetric heat capacity	$J\,K^{-1}\,m^{-3}$	1.35×10^5	Fitting
σ_{cn}	Electronic conductivity of copper negative current collector	$S\,m^{-1}$	5.96×10^7	Experiment
σ_{cp}	Electronic conductivity of aluminum positive current collector	$S\,m^{-1}$	3.77×10^7	Experiment

$$U(\text{SoC}, T) = \frac{dU}{dT}(T - T_{\text{ref}}) + 0.0027\,T\,I_{\text{sign}}$$
$$+ 3.382 + 0.0047\,\text{SoC} + 1.627\exp(-81.163\,\text{SoC}^{1.0138})$$
$$+ 7.6445 \times 10^{-8}\exp(25.36\,\text{SoC}^{2.469}) - 8.441 \times 10^{-8}$$
$$\times \exp(25.262\,\text{SoC}^{2.478}) - 3.3852 + 3.2585,$$

$$[\text{A·1}]$$

where $dU/dT = -10^{-4}$.

The initial conditions for the simulations are:

$$\text{SoC}(0) = \text{SoC}_0, \quad \text{on } \Omega \text{ and } \partial\Omega, \qquad [\text{A·2a}]$$

$$U(0) = U_0 = U(\text{SoC}_0), \quad \text{on } \Omega \text{ and } \partial\Omega, \qquad [\text{A·2b}]$$

$$V(y, z, 0) = V_0 = U_0 + R_0\,I_{\text{app}}, \quad \text{on } \Omega \text{ and } \partial\Omega, \qquad [\text{A·2c}]$$

$$v_1(y, z, 0) = 0, \quad \text{on } \Omega \text{ and } \partial\Omega, \qquad [\text{A·2d}]$$

$$v_2(y, z, 0) = 0, \quad \text{on } \Omega \text{ and } \partial\Omega, \qquad [\text{A·2e}]$$

$$T(y, z, 0) = T_{\text{ref}} = T_0, \quad \text{on } \Omega \text{ and } \partial\Omega. \qquad [\text{A·2f}]$$

ORCID

R. Drummond https://orcid.org/0000-0002-2586-1718
E. C. Tredenick https://orcid.org/0000-0001-9105-2858
T. L. Kirk https://orcid.org/0000-0002-6700-0852
M. Forghani https://orcid.org/0000-0003-2679-9060
P. S. Grant https://orcid.org/0000-0002-7942-7837
S. R. Duncan https://orcid.org/0000-0002-9525-7305

References

1. G. K. Singh, G. Ceder, and M. Z. Bazant, "Intercalation dynamics in rechargeable battery materials: General theory and phase-transformation waves in LiFePO₄." *Electrochimica Acta*, **53**, 7599 (2008).
2. E. C. Tredenick, S. Wheeler, R. Drummond, Y. Sun, S. R. Duncan, and P. S. Grant, "A Multilayer Doyle-Fuller-Newman model to optimise the rate performance of bilayer cathodes in Li Ion batteries." *J. Electrochem. Soc.*, **171**, 6 (2024).
3. A. S. Ho, D. Y. Parkinson, D. P. Finegan, S. E. Trask, A. N. Jansen, W. Tong, and N. P. Balsara, "3d detection of lithiation and lithium plating in graphite anodes during fast charging." *ACS Nano*, **15**, 10480 (2021).
4. S. N. Lauro, J. N. Burrow, and C. B. Mullins, "Restructuring the lithium-ion battery: A perspective on electrode architectures." *eScience*, 100152 (2023).
5. E. G. Sukenik, L. Kasaei, and G. G. Amatucci, "Impact of gradient porosity in ultrathick electrodes for lithium batteries." *J. Power Sources*, **579**, 233327 (2023).
6. R. Chowdhury, A. Banerjee, Y. Zhao, X. Liu, and N. Brandon, "Simulation of bi-layer cathode materials with experimentally validated parameters to improve ion diffusion and discharge capacity." *Sustainable Energy & Fuels*, **5**, 1103 (2021).
7. C. Cheng, R. Drummond, S. R. Duncan, and P. S. Grant, "Extending the energy-power balance of Li-ion batteries using graded electrodes with precise spatial control of local composition." *J. Power Sources*, **542**, 231758 (2022).
8. C. Cheng, R. Drummond, S. R. Duncan, and P. S. Grant, "Combining composition graded positive and negative electrodes for higher performance Li-ion batteries." *J. Power Sources*, **448**, 227376 (2020).
9. Z. Chen and Y. Zhao, "Tortuosity estimation and microstructure optimization of non-uniform porous heterogeneous electrodes." *J. Power Sources*, **596**, 234095 (2024).
10. S. H. Lee, C. Huang, and P. S. Grant, "Multi-layered composite electrodes of high power Li₄Ti₅O₁₂ and high capacity sno₂ for smart lithium ion storage." *Energy Storage Mater.*, **38**, 70 (2021).
11. S. Yari, H. Hamed, J. DHaen, M. K. Van Bael, F. U. Renner, A. Hardy, and M. Safari, "Constructive versus destructive heterogeneity in porous electrodes of lithium-ion batteries." *ACS Applied Energy Materials*, **3**, 11820 (2020).
12. A. M. Boyce, D. J. Cumming, C. Huang, S. P. Zankowski, P. S. Grant, D. J. Brett, and P. R. Shearing, "Design of scalable, next-generation thick electrodes: opportunities and challenges." *ACS Nano*, **15**, 18624 (2021).
13. E. C. Tredenick, A. M. Boyce, S. Wheeler, J. Li, Y. Sun, R. Drummond, S. R. Duncan, P. S. Grant, and P. R. Shearing, *Research Square* (2023), Bridging the gap between microstructurally resolved computed tomography-based and homogenised Doyle-Fuller-Newman models for lithium-ion batteries https://doi.org/10.21203/rs.3.rs-3639668/v1.
14. J. Wu, Z. Ju, X. Zhang, A. C. Marschilok, K. J. Takeuchi, H. Wang, E. S. Takeuchi, and G. Yu, "Gradient design for high-energy and high-power batteries." *Adv. Mater.*, **34**, 2202780 (2022).
15. R. Drummond, C. Cheng, P. S. Grant, and S. R. Duncan, "Modelling the impedance response of graded LiFePO₄ cathodes for Li-ion batteries." *J. Electrochem. Soc.*, **169**, 010528 (2022).
16. T. R. Garrick, Y. Zeng, J. B. Siegel, and V. R. Subramanian, "From atoms to wheels: The role of multi-scale modeling in the future of transportation electrification." *J. Electrochem. Soc.*, **170**, 113502 (2023).
17. V. Ramadesigan, R. N. Methekar, F. Latinwo, R. D. Braatz, and V. R. Subramanian, "Optimal porosity distribution for minimized ohmic drop across a porous electrode." *J. Electrochem. Soc.*, **157**, A1328 (2010).
18. S. Li, M. W. Marzook, C. Zhang, G. J. Offer, and M. Marinescu, "How to enable large format 4680 cylindrical lithium-ion batteries." *Appl. Energy*, **349**, 121548 (2023).
19. J. Liu, M. Kunz, K. Chen, N. Tamura, and T. J. Richardson, "Visualization of charge distribution in a lithium battery electrode." *The Journal of Physical Chemistry Letters*, **1**, 2120 (2010).
20. H. N. Chu, S. U. Kim, S. K. Rahimian, J. B. Siegel, and C. W. Monroe, "Parameterization of prismatic lithium–iron–phosphate cells through a streamlined thermal/electrochemical model." *J. Power Sources*, **453**, 227787 (2020).
21. J. Lin, H. N. Chu, D. A. Howey, and C. W. Monroe, "Multiscale coupling of surface temperature with solid diffusion in large lithium-ion pouch cells." *Commun. Eng.*, **1**, 1 (2022).
22. A. Mikheenkova, A. Schökel, A. J. Smith, I. Ahmed, W. R. Brant, M. J. Lacey, and M. Hahlin, "Visualizing ageing-induced heterogeneity within large prismatic lithium-ion batteries for electric cars using diffraction radiography." *J. Power Sources*, **599**, 234190 (2024).
23. A. Fordham et al., "Correlative non-destructive techniques to investigate aging and orientation effects in automotive Li-ion pouch cells." *Joule*, **7**, 2622 (2023).
24. S. Yari, M. K. Van Bael, A. Hardy, and M. Safari, "Non-uniform distribution of current in plane of large-area lithium electrodes." *Batteries & Supercaps*, **5**, e202200217 (2022).
25. X.-G. Yang, T. Liu, Y. Gao, S. Ge, Y. Leng, D. Wang, and C.-Y. Wang, "Asymmetric temperature modulation for extreme fast charging of lithium-ion batteries." *Joule*, **3**, 3002 (2019).
26. M. G. Bason, T. Coussens, M. Withers, C. Abel, G. Kendall, P. Krüger, and , "Non-invasive current density imaging of lithium-ion batteries." *J. Power Sources*, **533**, 231312 (2022).
27. M. Mohammadi, E. V. Silletta, A. J. Ilott, and A. Jerschow, "Diagnosing current distributions in batteries with magnetic resonance imaging." *J. Magn. Reson.*, **309**, 106601 (2019).
28. Z. Wang, D. L. Danilov, R.-A. Eichel, and P. H. Notten, "About the in-plane distribution of the reaction rate in lithium-ion batteries." *Electrochim. Acta*, **475**, 143582 (2024).
29. M. Yazdanpour, P. Taheri, A. Mansouri, and M. Bahrami, "A distributed analytical electro-thermal model for pouch-type lithium-ion batteries." *J. Electrochem. Soc.*, **161**, A1953 (2014).
30. J. M. Campillo-Robles, X. Artetxe, and K. del Teso Sánchez, "Effect of thickness on the maximum potential drop of current collectors." *Appl. Phys. Lett.*, **111** (2017).
31. C. Cho, S. Kelley, J. G. Tylka, M. He, N. N. Nandola, and C. D. Rahn, "Improving nonuniform utilization of Li-ion pouch cells using tapered electrodes through calendering." *International Design Engineering Technical Conferences and Computers and Information in Engineering Conference* Vol. 87301 (American Society of Mechanical Engineers) (2023).
32. P. Taheri, A. Mansouri, M. Yazdanpour, and M. Bahrami, "Theoretical analysis of potential and current distributions in planar electrodes of lithium-ion batteries." *Electrochim. Acta*, **133**, 197 (2014).
33. J. Newman and W. Tiedemann, "Potential and current distribution in electrochemical cells: Interpretation of the half-cell voltage measurements as a function of reference-electrode location." *J. Electrochem. Soc.*, **140**, 1961 (1993).
34. M. Parmananda, B. S. Vishnugopi, H. Garg, and P. P. Mukherjee, "Underpinnings of multiscale interactions and heterogeneities in Li-ion batteries: Electrode microstructure to cell format." *Energy Technology*, **11**, 2200691 (2023).
35. Y. Hahn, Z. Gao, T.-T. Nguyen, and V. Oancea, "A reduced order model for a lithium-ion 3D pouch battery for coupled thermal-electrochemical analysis." *Journal of Energy Storage*, **70**, 107966 (2023).
36. M. Guo, G.-H. Kim, and R. E. White, "A three-dimensional multi-physics model for a Li-ion battery." *J. Power Sources*, **240**, 80 (2013).
37. Y.-W. Pan, Y. Hua, S. Zhou, R. He, Y. Zhang, S. Yang, X. Liu, Y. Lian, X. Yan, and B. Wu, "A computational multi-node electro-thermal model for large prismatic lithium-ion batteries." *J. Power Sources*, **459**, 228070 (2020).
38. R. C. Aylagas, C. Ganuza, R. Parra, M. Yañez, and E. Ayerbe, "cideMOD: An open source tool for battery cell inhomogeneous performance understanding." *J. Electrochem. Soc.*, **169**, 090528 (2022).
39. M. Doyle, T. F. Fuller, and J. Newman, "Modeling of galvanostatic charge and discharge of the lithium/polymer/insertion cell." *J. Electrochem. Soc.*, **140**, 1526 (1993).
40. S. Santhanagopalan, Q. Guo, P. Ramadass, and R. E. White, "Review of models for predicting the cycling performance of lithium ion batteries." *J. Power Sources*, **156**, 620 (2006).
41. E. Hosseinzadeh, J. Marco, and P. Jennings, "The impact of multi-layered porosity distribution on the performance of a lithium ion battery." *Appl. Math. Modelling*, **61**, 107 (2018).
42. J. T. Frith, M. J. Lacey, and U. Ulissi, "A non-academic perspective on the future of lithium-based batteries." *Nat. Commun.*, **14**, 420 (2023).
43. G. L. Plett, *Battery Management Systems, Volume II: Equivalent-circuit Methods* (Artech House) (2015).
44. L. N. Trefethen, *Spectral methods in MATLAB* (SIAM, Philadelphia) (2000).
45. (MATLAB), *Version 9.13 (R2022b)* (The MathWorks Inc.) (2022).
46. S. E. O'Kane, W. Ai, G. Madabattula, D. Alonso-Alvarez, R. Timms, V. Sulzer, J. S. Edge, B. Wu, G. J. Offer, and M. Marinescu, "Lithium-ion battery degradation: how to model it." *Phys. Chem. Chem. Phys.*, **24**, 7909 (2022).
47. J. M. Reniers, G. Mulder, and D. A. Howey, "Review and performance comparison of mechanical-chemical degradation models for lithium-ion batteries." *J. Electrochem. Soc.*, **166**, A3189 (2019).
48. L. D. Couto, R. Romagnoli, S. Park, D. Zhang, S. J. Moura, M. Kinnaert, and E. Garone, "Faster and healthier charging of lithium-ion batteries via constrained feedback control." *IEEE Trans. Control Syst. Technol.*, **30**, 1990 (2021).
49. R. Romagnoli, L. D. Couto, A. Goldar, M. Kinnaert, and E. Garone, "A feedback charge strategy for Li-ion battery cells based on reference governor." *J. Process Control*, **83**, 164 (2019).
50. V. Zinth, C. Von Lüders, M. Hofmann, J. Hattendorff, I. Buchberger, S. Erhard, J. Rebelo-Kornmeier, A. Jossen, and R. Gilles, "Lithium plating in lithium-ion

batteries at sub-ambient temperatures investigated by in situ neutron diffraction." *J. Power Sources*, **271**, 152 (2014).

51. J. Burns, D. Stevens, and J. Dahn, "In-situ detection of lithium plating using high precision coulometry." *J. Electrochem. Soc.*, **162**, A959 (2015).

52. P. M. Attia et al., "Closed-loop optimization of fast-charging protocols for batteries with machine learning." *Nature*, **578**, 397 (2020).

53. G. Tucker, R. Drummond, and S. R. Duncan, "Optimal fast charging of lithium ion batteries: Between model-based and data-driven methods." *J. Electrochem. Soc.*, **170**, 120508 (2023).

54. A. G. Kashkooli, S. Farhad, D. U. Lee, K. Feng, S. Litster, S. K. Babu, L. Zhu, and Z. Chen, "Multiscale modeling of lithium-ion battery electrodes based on nano-scale x-ray computed tomography." *J. Power Sources*, **307**, 496 (2016).